Order, disorder, and metalation of tetraphenylporphyrin (2H-TPP) on Au(111)

Matthew Edmondson[1], Eleanor S. Frampton[1,2], Chris J. Judd[1], Neil R. Champness[3], Robert G. Jones[2], Alex Saywell[1]*

[1]School of Physics & Astronomy, The University of Nottingham, Nottingham, NG7 2RD, UK.

[2]School of Chemistry, The University of Nottingham, Nottingham, NG7 2RD, UK.

*Corresponding author A.S. (Alex.Saywell@nottingham.ac.uk)

Supporting Information

Contents

Experimental Methods....2
STM characterisation of close-pack assemblies of 2H-TPP....5
2H-TPP adsorption at step-edges....8
STM characterisation of 'diffuse' phase of 2H-TPP on Au(111)....9
Details of the molecular density for close-packed and 'diffuse' phases of 2H-TPP on Au(111)....10
Details of the cyclodehydrogenation of 2H-TPP on Au(111)....11
STS analysis of 2H-TPP assemblies on Au(111)....12
XPS peak fitting details....14
NEXAFS characterisation....15
References....19

Experimental Methods

STM

Scanning tunnelling microscopy (STM) experiments were performed using a Scienta Omicron low temperature (LT) STM system, CreaTec LT STM system and a Scienta Omicron POLAR LT STM system, operating under ultra-high vacuum (UHV) conditions with base pressures of better than $3x10^{-10}$ mbar. Images were acquired at cryogenic temperatures (~80K and ~6.5 K - CreaTec, or ~78K and ~4.7 K, Scienta Omicron) in constant current mode using electrochemically etched tungsten tips, coated in gold during tip optimisation by controlled indentation into the surface.

STM experiments were carried out on the CreaTec system using Au(111) on mica substrates (Georg Albert PVD GmbH) prepared by cycles of Ar ion sputtering for 30 minutes at 0.6 keV, followed by annealing at 870 K for 30 minutes. Sample temperatures were estimated based on pyrometer measurements; the associated uncertainty for temperature measurements is estimated to be ± 50K.

STM experiments were carried out on the Scienta Omicron LT system using a Au(111) single crystal substrate (MaTeck GmbH) prepared by cycles of Ar ion sputtering for 30 minutes at 1.0 keV, followed by annealing at 740 K for 30 minutes. Sample temperature was estimated based on pyrometer measurements; the associated uncertainty for temperature measurements is estimated to be ± 50K.

STM experiments were carried out on the Scienta Omicron POLAR system using a Au(111) single crystal substrate (Surface Preparation Laboratory) prepared by cycles of Ar ion sputtering for 30 minutes at 1.0 keV, followed by annealing at 790 K for 30 minutes.

2H-TPP was synthesised using a previously described method.[1] Molecules were deposited onto a Au(111) surface held at room temperature using a Knudsen cell heated to ~230^{o}C. Coverage of 2H-TPP was altered by increasing/decreasing deposition time following surface cleaning.

XPS, NEXAFS and LEED (I09 beamline at Diamond Light Source)

A clean Au(111) substrate was prepared via several sputter-anneal cycles under UHV conditions (sputter: 1 keV for 30 minutes, annealing to 690 K for 30 minutes) and was subsequently characterised by LEED and XPS. The clean Au(111) surface was then exposed to a flux of 2H-TPP produced via sublimation from a Knudsen-type evaporator (280°C for 30 minutes, substrate held at room temperature). Sample temperatures were estimated based on calibration data obtained from a thermocouple positioned on a dummy sample; the associated uncertainty for temperature measurements is estimated to be ± 50K.

The various phases of 2H-TPP (close-packed, diffuse, and metalated) were obtained via systematically heating the substrate to elevated temperatures. For each phase, characterisation was performed using LEED, XPS (C1s and N1s regions) and NEXAFS (N1s K-edge). Measurements were performed at Diamond Light Source (I09)[2] with samples held at room temperature and ultra-high vacuum (UHV); base pressure 4×10^{-10} mbar. The I09 beamline consists of two undulator light sources that separately cover “soft” (100-2000 eV) and “hard” (2100 – 15000 eV) X-ray energy ranges. The photoelectron spectra were acquired using a VG Scienta EW4000 HAXPES analyser that was mounted perpendicular to the incident light in the same plane as the photon polarization (linear horizontal).

LEED characterisation was performed at energies of 6.5, 15.5, 22.5, and 66.5 eV. High-resolution C1s and N1s XPS measurements were acquired using the soft X-ray (SXR)

undulator on the I09 beamline, acquired at 900 eV and 600 eV respectively. Angle dependent NEXAFS data were acquired at normal incidence (0^o), grazing incidence (85^o), and 55^o ('magic angle'). Long exposure to the beam could cause beam damage, however, the incoming X-ray was detuned to reduce the intensity on the sample. All measurements were carried out with the sample held at RT and all measurements were acquired at different locations on the sample.

STM characterisation of close-pack assemblies of 2H-TPP

Details of close-packed assemblies of 2H-TPP on Au(111) as characterised by low-temperature STM measurements.

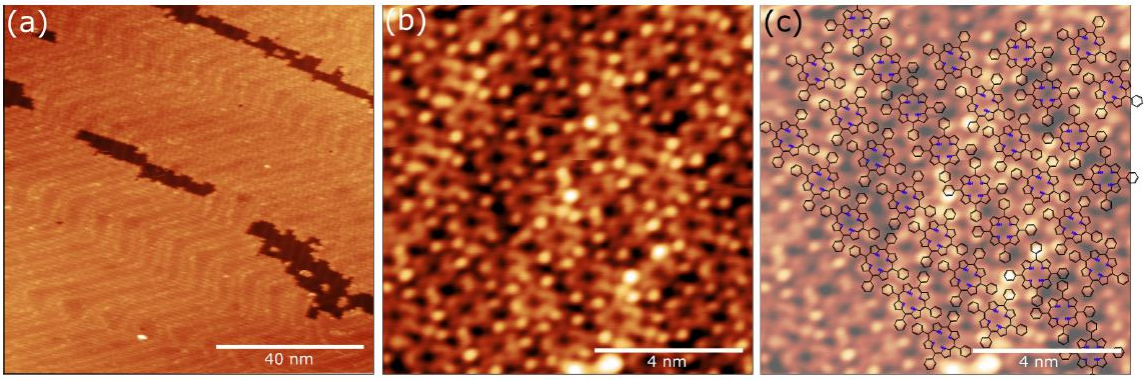

Figure S1. STM images showing close-packed assemblies of 2H-TPP on Au(111). (a) Overview image showing large islands of TPP, with the underlying herringbone reconstruction of the surface visible. (b) Image showing sub-molecular resolution within a close-packed island of 2H-TPP, with the corresponding molecular positions indicated in (c). [Image parameters: (a) V_{sample} = -0.8 V, $I_{set\text{-}point}$ = 30 pA. (b) V_{sample} = 1.2 V, $I_{set\text{-}point}$ = 50 pA, T_{sample}=80 K.]

Within close-packed islands, 'rows' of 2H-TPP are observed, with 2H-TPP molecules in neighbouring rows observed to be rotated at an angle of ~30° relative to each other in some instances (see green and blue boxes in Figure S2 – 'row' direction indicated by red lines).

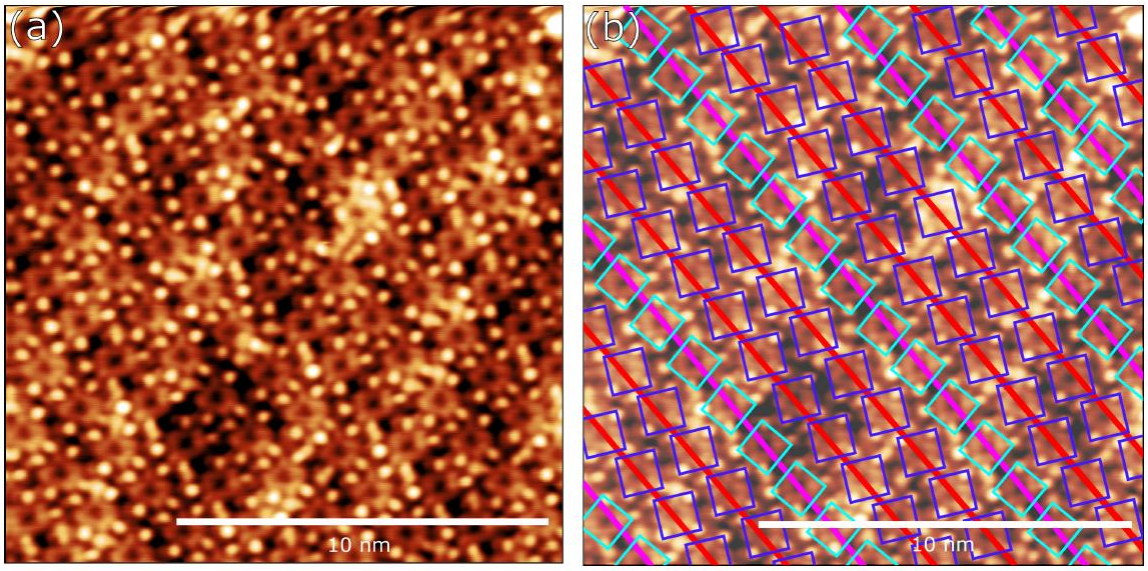

Figure S2. (a) STM image showing close-packed assemblies of 2H-TPP on Au(111) with molecular rotation exhibited in some rows, as shown in (b). (b) STM image with row directions indicated with red lines and two molecular orientations shown with green and blue boxes (rotated by 30° relative to each other) [Image parameters: (a,b) V_{sample} = 0.6 V, $I_{set\text{-}point}$ = 50 pA, T_{sample}=80 K.]

The STM analysis of the unit-mesh for the close-packed structure can be defined within domains containing 2H-TPP in one rotational orientation to be 1.62 ± 0.06 nm by 1.44 ± 0.01 nm with an internal angle of 105±20°. In a mixed domain (considering alternating rows of rotated 2H-TPP) the unit-mesh is slightly enlarged between the rows and was found to be 1.90 ± 0.01 nm by 1.43 ± 0.01 nm with an internal angle of 124±20°.

Based upon LEED analysis of the close-packed phase (see Figure 1e in the manuscript), we obtain the matrix description of an incommensurate overlayer:

$$\begin{pmatrix} 3.96 & 5.41 \\ -3.96 & 1.45 \end{pmatrix}$$

Figure S3 shows the unit-mesh this overlayer on a (111) surface plane. This corresponds to a square overlayer structure with dimensions 1.4 ± 0.1 nm by 1.4 ± 0.1 nm (with an internal angle of 90°). The errors represent the fact that similar LEED patterns may be generated using square lattices of slightly different dimensions.

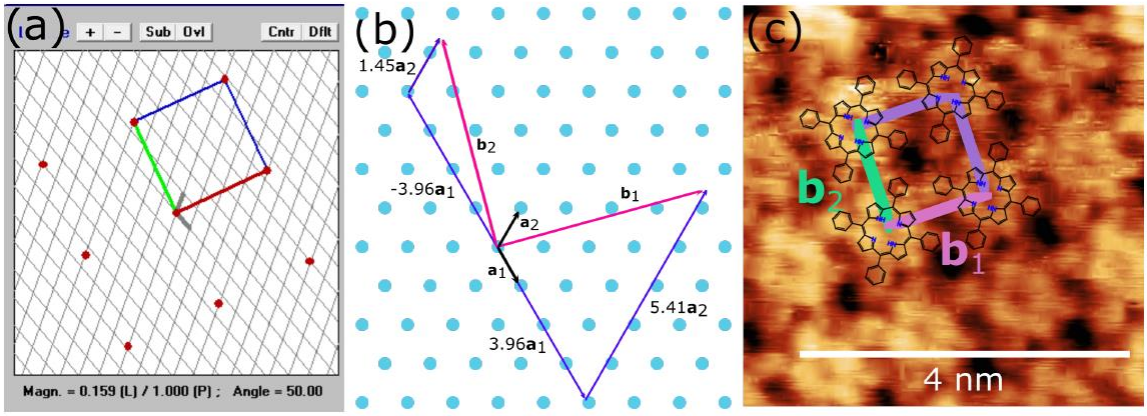

Figure S3. Schematics showing the dimensions of the close-packed 2H-TPP unit-mesh based upon analysis of LEED data. (a) Square lattice generated from the overlayer matrix shown above. (b) Scheme showing substrate and overlayer vectors. (c) Scale model showing unit-mesh of LEED-based overlayer structure superimposed upon an STM image of a close-packed domain of 2H-TPP. [Image parameters: (c) V_{sample} = 1.8 V, $I_{set\text{-}point}$ = 100 pA, T_{sample}=80 K.]

We note that the STM images shown in Figures S1 and S2 do not show the same 'square' lattice as that described by the LEED data, however, this is possible due to a number of

factors such as a variety of packing motifs and drift present within the STM image. The STM image, in Figure S3c, shows a square close-packed structure where drift was reduced by scanning in the same area for a prolonged period, and a packing structure that matches the LEED data.

Scanning probe microscopy (SPM) techniques give very high lateral resolution, particularly in the 'fast-scan' direction, however due to thermal drift (and/or piezoelectric creep) SPM characterisation can be sub-optimal for angular measurements: These factors result in a distortion of the image, particularly along the 'slow-scan' axis, and will consequently distort the angle measured within the unit-mesh. LEED analysis can be used to provide a spatially averaged value of the mesh but does not account for local variations, for example in the instance in which the two orientations of the TPP molecule were present in alternating rows. The two techniques should therefore be used in tandem to gain access to accurate unit-mesh dimensions as deduced from the LEED pattern, and the local information gained from the STM images.

2H-TPP adsorption at step-edges

Following deposition onto Au(111), 2H-TPP is observed to adsorb at step-edges. This is a preferential adsorption site as indicated by the decoration of the step edges at low coverages (Fig. S4a). From a comparison of several sub-monolayer coverages, it is evident that decoration of the step edges occurs prior to nucleation of 2H-TPP at all the available elbow sites of the herringbone reconstruction. At higher coverages, island growth is observed.

High-resolution STM images (Fig. S4b) show that the core of the 2H-TPP molecule is adsorbed above the low-coordinated Au atoms within the step edge. This results in the phenyl 'legs' of the 2H-TPP being observed on both upper and lower terraces adjacent to the step-edge.

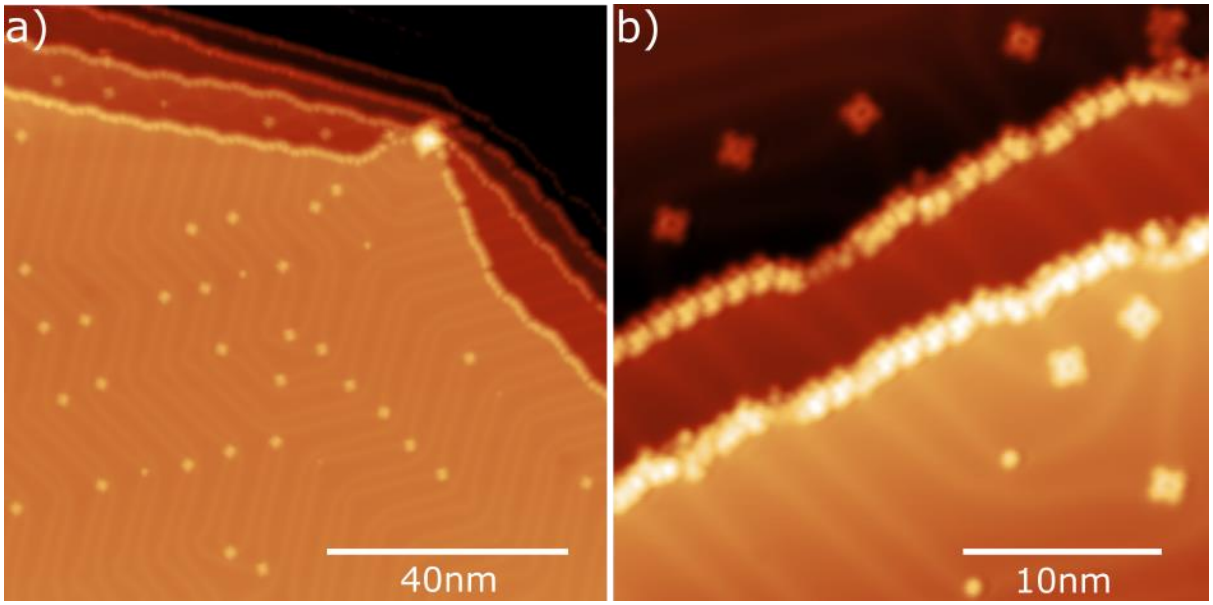

Figure S4. STM images showing the adsorption of 2H-TPP at the step-edges of the Au(111) surface. The 2H-TPP used in these images was acquired from Sigma-Aldrich (>99% purity). [Image parameters: (a) V_{sample} = -1.8 V, $I_{set\text{-}point}$ = 50 pA, T_{sample}= 4.7 K. (b) V_{sample} = 1.0 V, $I_{set\text{-}point}$ = 50 pA, T_{sample}=4.7 K]

STM characterisation of 'diffuse' phase of 2H-TPP on Au(111)

Preparation of a sub-monolayer (ML) coverage of 2H-TPP on the Au(111) surface results in the formation of small islands (2-9 molecules per island) of 2H-TPP. The arrangement of molecules within the islands is found to be a similar arrangement as for the close-packed islands observed for the ~1 ML coverage (with molecules observed in a mixture of the two rotations discussed in Figure S2). Dimers are found to be the most commonly occurring species, with preferential adsorption at the FCC regions of the herringbone reconstruction being identified.[3] Figure S5 shows the change in molecular positioning following annealing to 580 ± 50 K. Isolated molecules are now present, with the preferential adsorption location still being the FCC regions of the herringbone reconstruction.

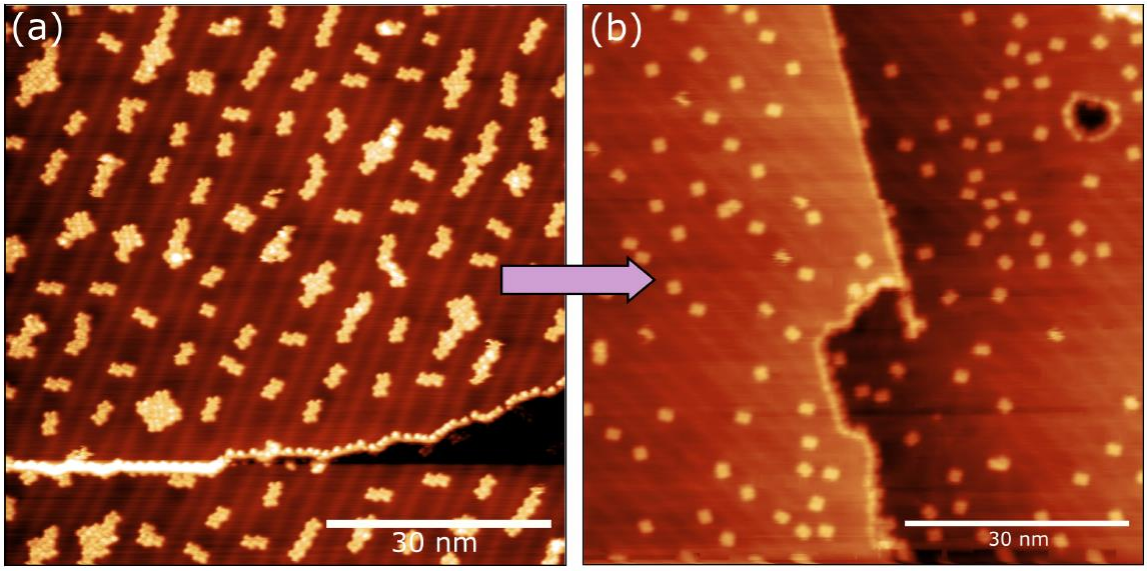

Figure S5. (a) STM image showing the close-packed structures formed for a sub-monolayer coverage of 2H-TPP on a Au(111) surface. (b) STM image showing the observed change in molecular assembly following annealing of the surface at 580 ± 50 K. Image parameters: (a) V_{sample} = -1.3 V, $I_{set\text{-}point}$ = 25 pA. (b) V_{sample} = 1.3 V, $I_{set\text{-}point}$ = 25 pA, T_{sample}=6.5 K.]

Details of the molecular density for close-packed and 'diffuse' phases of 2H-TPP on Au(111)

Based upon the LEED data acquired for the close-packed and 'diffuse' phases of 2H-TPP we are able to calculate the density of molecular species present. As the LEED data for the diffuse phase provides an average molecule-molecule separation, we will assume a square unit cell with sides equal to this separation in order to facilitate comparison with square unit cell determined from the LEED measurements of the close-packed structures.

Table 1: Molecule-molecule separations, obtained from LEED measurements, for TPP in the close-packed and diffuse phases. Estimated unit cell areas and molecular densities are calculated as described in the text.

Phase	Molecule-Molecule separation (nm)	Estimated unit cell area (nm^2)	Molecular density (molecules per nm^2)
Close-packed	1.40 ± 0.1	2.0 ± 0.2	0.51 ± 0.05
Diffuse	1.52 ± 0.1	2.3 ± 0.2	0.43 ± 0.04

Details of the cyclodehydrogenation of 2H-TPP on Au(111)

Following annealing of the close-packed phase of 2H-TPP a diffuse phase is produced (see Figure S6). The structure of 2H-TPP observed within the STM images is different to that apparent in the close-packed structures, and is consistent with 'flattening' or 'distortion' of the molecule induced by an on-surface cyclodehydrogenation reaction (multiple, frequently 4, cyclodehydrogenations per molecules), as previously reported upon.[4–6]

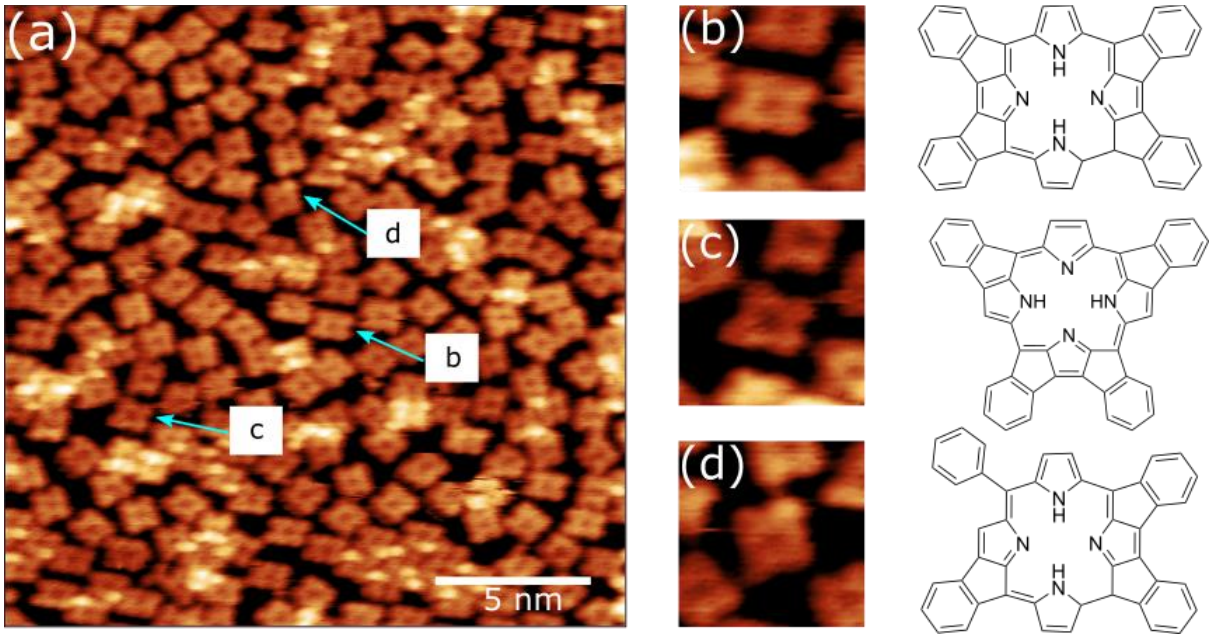

Figure S6. (a) STM image showing the observed change in the structure of the 2H-TPP species within the diffuse phase following annealing of the surface at 580 ± 50 K. (b-c) Regions of the STM image in (a) highlighting the appearance of the 2H-TPP with corresponding tentative structural models based upon potential cyclisation products. Image parameters: (a,b) V_{sample} = 1.3 V, $I_{set\text{-}point}$ = 5 pA, T_{sample}=6.5 K.]

STS analysis of 2H-TPP assemblies on Au(111)

Scanning tunnelling spectroscopy (STS) measurements were acquired to obtain information relating to the electronic structure of the 2H-TPP molecules present on the Au(111) surface. The data is presented as differential conductance (dI/dV) as a function of voltage (V – bias applied to sample) with the resonances ('peaks') observed assigned to specific electronic features. In the case of 2H-TPP on Au(111), resonances have previously been assigned to both the highest occupied molecular orbital (HOMO) and the lowest unoccupied molecular orbital (LUMO).[7]

Figure S7 shows an STS spectrum acquired over a 2H-TPP molecule on the Au(111) surface, with resonances observed at -1.1 V and + 1.6 V (a smaller resonance is also found at around -0.4 V and is assigned to a surface state). Based on previous work, we assign the peaks at -1.1 V and + 1.6 V to the HOMO and LUMO, respectively.[7]

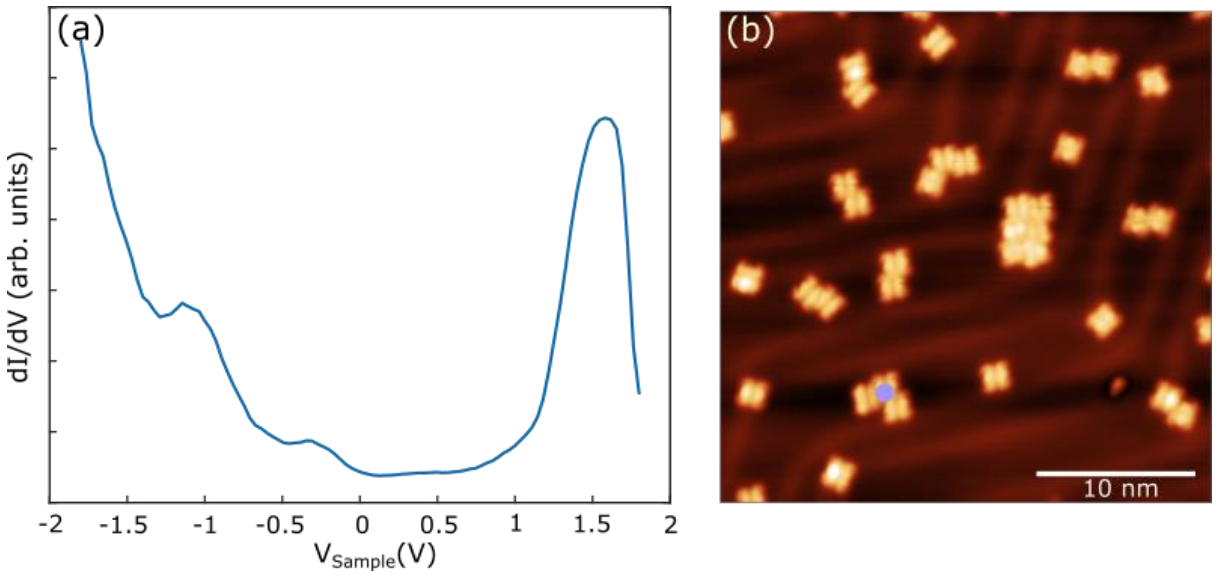

Figure S7. (a) STS spectrum for a 2H-TPP species on Au(111). (b) STM image of 2H-TPP on Au(111) with the purple dot indicating the position where the STS spectrum was acquired. Image parameters: (b) V_{sample} = -1.8 V, $I_{set\text{-}point}$ = 80 pA, T_{sample}=6.5 K.]

For the same surface preparation, we also identify 2H-TPP species where the STS resonances for the HOMO and LUMO are observed at different bias voltages. Figure S8a shows two STS spectra for two distinct 2H-TPP species (labelled here as Type 1 and Type 2). Type 1 is identified as 2H-TPP, and the relative abundance for Type 1 and Type 2 are

92% and 8 %, respectively. Based upon the STM, STS, and density functional theory (DFT) analysis of Mielke *et al.*[7] we attribute the Type 2 species to a 2H-TPP interacting with a Au adatom (compare Figures S8a and S8b). The position of the peaks assigned to the HOMO and LUMO for the Type 2 species (-1.7 V and + 1V – NB bias voltage in Figure S8a is defined relative to the tip to allow comparison with the published results shown in Figure S8b) are shifted by approximately 0.5 V relative to Type 1, with the magnitude of the HOMO-LUMO separation remaining at 2.5 eV for both Type 1 and Type 2.

Additionally, we find that the frequency of occurrence of Type 1 and Type 2 molecules is altered following annealing the Au substrate (with an increase in the Type 2, adatom-2H-TPP, species observed). This finding is in good agreement with the expectation that annealing the substrate should result in an increase in the availability of Au adatom species (e.g. diffusion from step-edges) and therefore facilitate the formation of additional adatom-2H-TPP. This effect is also observed in the N1s X-ray photoelectron spectroscopy (XPS) as discussed in the main manuscript.

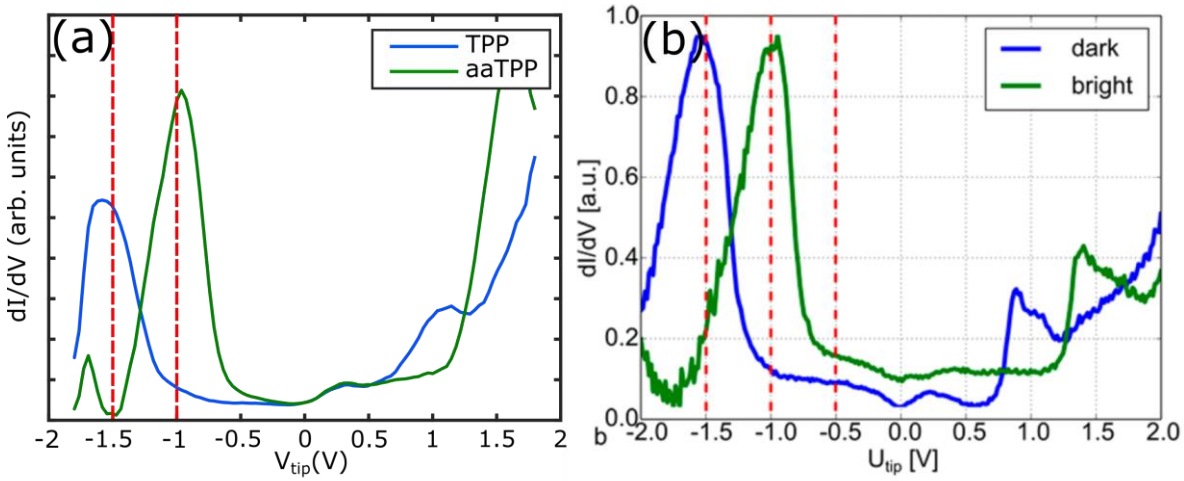

Figure S8. (a) STS spectra for Type 1 (2H-TPP, blue) and Type 2 (adatom-2H-TPP, green) species on Au(111). (b) STS data for 2H-TPP and adatom-2H-TPP as published by Mielke et al.[7] showing resonances (assigned to HOMO and LUMO features) in agreement with the STS data acquired within this work. [Figure 7(b) reproduced with permission under a Creative Commons license from ref. 7, Copyright 2014.]

XPS peak fitting details

The N1s and C1s XP spectra of each phase (close-packed, diffuse and metalated) were obtained and show the chemical state of the TPP species on the Au(111) surface in each phase. The binding energies (BE) were calibrated to the fermi level of the Au(111) surface.

The N1s spectra peak assignments, listed in Table 2, showed the expected iminic and pyrrolic peaks, each with an additional feature at slightly higher BE which we attribute to an interaction with Au adatoms as seen in our STM data and previously published work.[7] Upon annealing to produce the diffuse phase, there was no significant change to the peak position, with only a reduction in the intensity of the (N/NH) Au adatom interaction. Further annealing formed a single feature (indicative of metalation of TPP) with smaller residual iminic and pyrrolic features attributed to incomplete metalation of the TPP species.

The peaks were fitted using a linear background subtraction and Doniach Sunjic line shapes (asymmetry factors of 0.05, 0.15, and 0.05 for, respectively, the close-packed, diffuse, and metalated phases). The peak widths are all in the range 0.7-0.9 eV FWHM (full width at half maximum). The peak assigned to the 'metalated' (Au-N) interaction could conceivably contain two peaks of approximately equal intensity separated by ~0.2 eV (which would lead to an enhanced fit).

We propose that the increase in asymmetry factor, which is observed for the diffuse phase (asymmetry - 0.15), is due to an increased interaction with the Au(111) surface as compared to the close-packed and metalated phases (asymmetry - 0.05). The three different phases of TPP have the potential to exhibit varying levels of interaction with the electronic states of the gold surface. Our model, based upon the STM and C1s XPS data presented within the manuscript, allows us to state that TPP within the close-packed phase exists in a non-planar saddle shape (see, for example, reference 7). TPP species within the diffuse phase have undergone a cyclisation reaction, and as such the atoms within the molecule will be quasi-coplanar; potentially facilitating a greater hybridisation between

molecular states and those of the Au substrate. Additionally, the metalated phase is likely to be comparatively decoupled (as compared to the diffuse phase) from the surface as the inclusion of a Au adatom within the porphyrin macrocycle would result in an increased separation between the TPP species and the top layer of the gold surface. We suggest that the interaction between molecule and surface surface (which is likely to be increased for the diffuse phase) provides access to energy loss mechanisms (with electrons being excited to the continuum of empty states associated with the Au substrate) giving rise to an expected asymmetry in the peaks which we account for by fitting the data using Doniach-Sunjic line shapes.

Table 2: N1s fitted peak binding energies.

Surface preparation	Iminic (=N-) (eV)	Iminic (=N-) + Au interaction (eV)	Pyrrolic (-NH-) (eV)	Pyrrolic (-NH-) + Au interaction (eV)	Metalated (Au-N) (eV)
Close-packed	397.2	397.7	399.3	400.0	
Diffuse	397.4	397.7	399.2	399.9	
Metalated	397.4		399.2	400.0	398.0

The close-packed C1s spectra peak assignments, listed in Table 3, were made using work previously carried out by Nardi *et al.*.[8] A combination of four environments were fitted to the data with a shakeup feature present at a higher binding energy.

Table 3: C1s Close-packed binding energies for each environment.

C1s Environment	Binding Energy (eV)
C_{Ph}	284.1
C^{B}_{α} & C_{m}	284.7
C^{A}_{α}	285.5
C^{A}_{β} & C^{B}_{β}	283.9
Shakeup	~287

NEXAFS characterisation

NEXAFS data was acquired for the nitrogen K-edge for the three phases of 2H-TPP on Au(111). The data was normalised using methods described by Watts *et al*.[9]

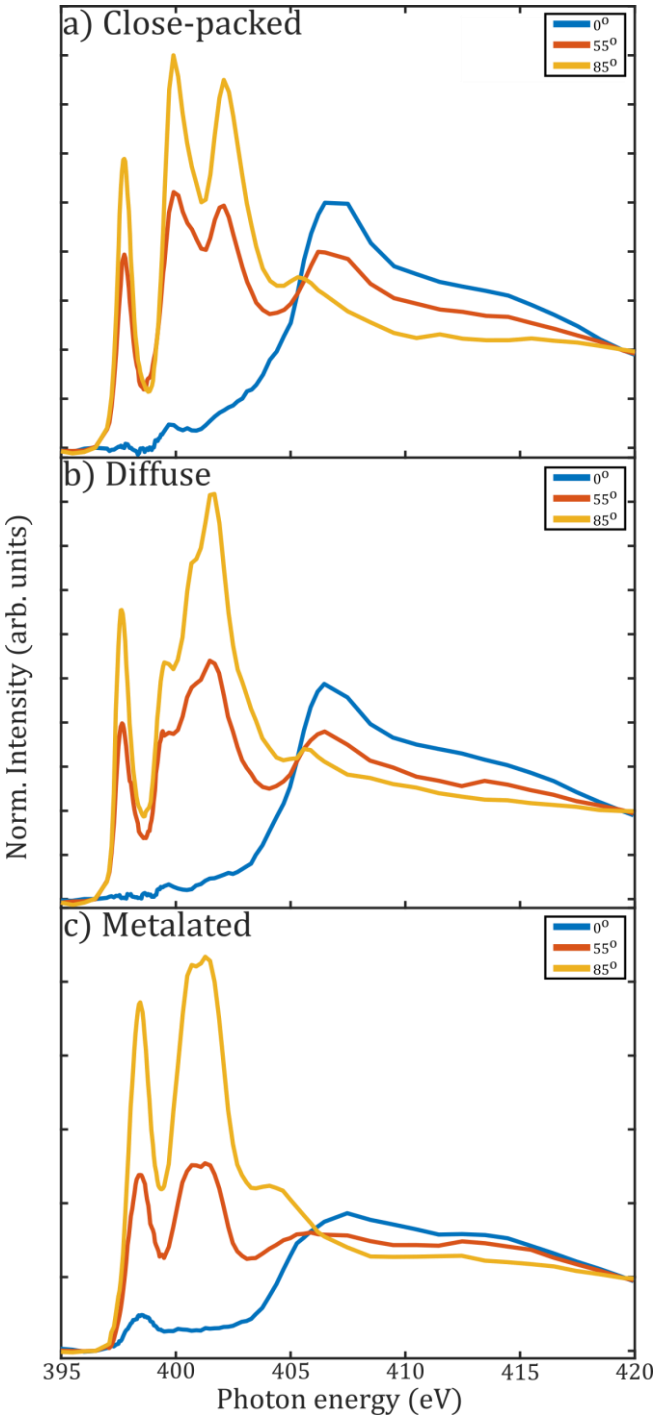

Figure S9. NEXAFS spectra acquired at normal incidence (0°), 'magic angle' (55°) and grazing incidence (85°) orientations for (a) the close-packed phase, (b) the diffuse phase, and (c) the metalated phase.

The NEXAFS data may be used to provide a 'fingerprint' of the metalated TPP species. Following metalation, there is a clear change in the dichroism of the first peak (close-packed 397.8eV and metalated 398.4eV) for the normal incidence spectra. This indicates that the macrocycle is tilted slightly following metalation.[10] The resonances in NEXAFS provide information on the unoccupied states of the molecular species under study. In Figure S10 we offer a comparison between our studies of 2H-TPP on Au(111) and previous work on the self-metalation of 2H-TPP on the Cu(111) surface reported by Diller *et al*.[11] where DFT calculations are compared to experimental NEXAFS spectra.

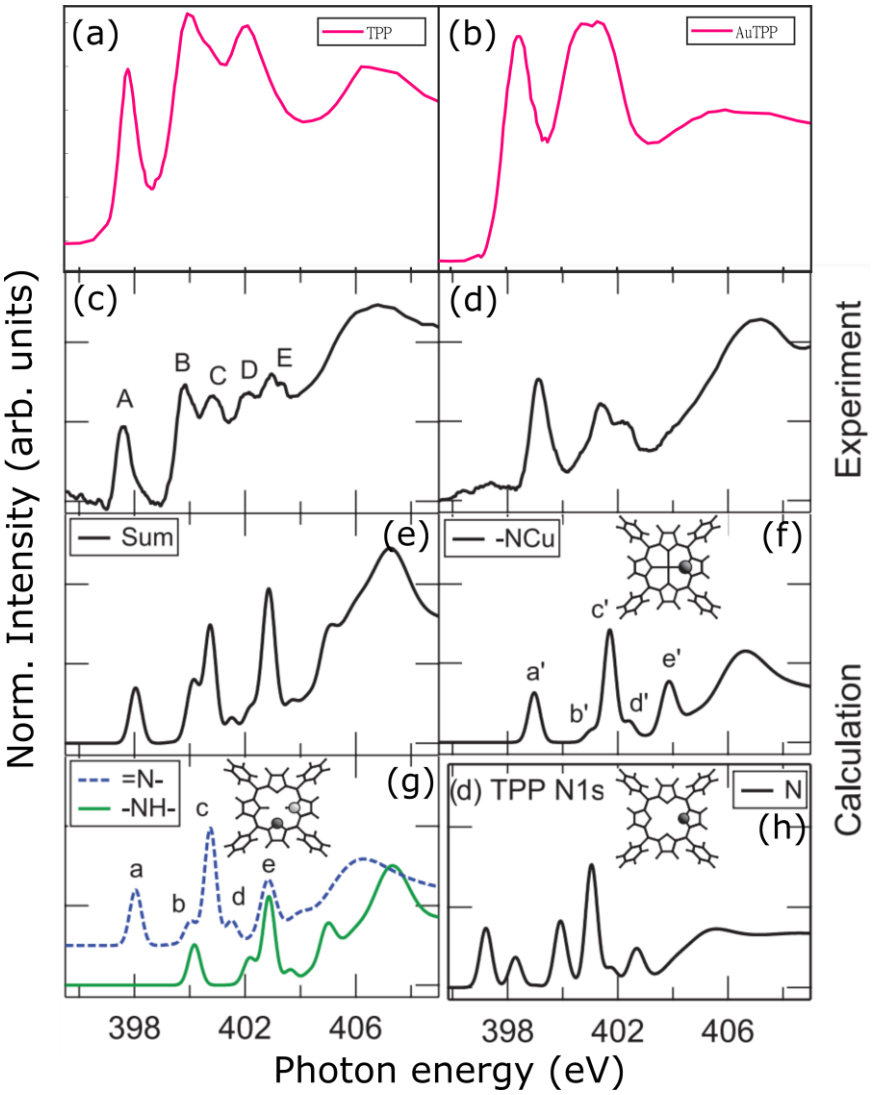

Figure S10. NEXAFS for the nitrogen K-edge region acquired for 2H-TPP on Au(111) with an angle of incidence of (55°), for (a) a close-packed phase, and (b) a metalated phase. (c-h) Experimentally obtained and DFT calculated nitrogen K-edge NEXAFS reproduced from Ref [11]: Experimental data for (c) 2H-TPP on Cu(111) and (d) Cu-TPP on Cu(111). Calculated spectra for (e) 2H-TPP, (f) Cu-TPP, (g) Cu-TPP with contribution from iminic (N) and pyrrolic

(NH) nitrogen species indicated, and (h) the deprotonated TPP species. [Figure 8(c-h) reprinted from Diller, K.; Klappenberger, F.; Marschall, M.; Hermann, K.; Nefedov, A.; Wöll, Ch.; Barth, J. V. *J. Chem. Phys.* **2012**, *136* (1), 014705, with the permission of AIP Publishing.]

The NEXAFS data for the 2H-TPP species in our study (Fig. S9a) matches well with that reported for 2H-TPP on Cu(111)[11] (Fig. S9c), with resonances at 397.8 eV and 397.6 eV, respectively (which is attributed to a π^* transition). The calculated NEXAFS data (Fig. S9e) is also in good agreement with our experimental data, showing broad peaks at ~400 eV and ~402 eV and a σ^* feature at ~407 eV.

We also observe a good agreement between the metalated Cu-TPP species and the species which we label as Au-TPP (compare Figure S10b and S10d). The observed peaks are also reproduced in the calculated NEXAFS data (Figure S10f). Importantly, there is little to no agreement with the calculated spectra for a deprotonated TPP species (Figure S10h). This indicates that the single nitrogen environment observed within the XPS data (Figure 3a) may be more readily attributed to Au-TPP and not a deprotonated TPP species. The peaks present in our NEXAFS data and the Cu(111) experiment/DFT peaks are displayed in Table 4.

Table 4: NEXAFS peak positions [#This work, * Data reproduced from Diller *et al*.[11]]

Phase	Source	Peak 1	Peak 2	Peak 3	Peak 4
Close-Packed	Au(111) Exp#	397.8	399.9	401.9	406.5
	Cu(111) Exp*	397.6	399.8	401.6	
	Cu(111) DFT*	398.0	400.0	402.2	
Metalated	Au(111) Exp#	398.4	400.7	401.3	407.5
	Cu(111) Exp*	398.4	400.7	401.3	405.3
	Cu(111) DFT*	398.5	400.7	401.3	404.1

References

(1) Lindsey, J. S.; Schreiman, I. C.; Hsu, H. C.; Kearney, P. C.; Marguerettaz, A. M. Rothemund and Adler-Longo Reactions Revisited: Synthesis of Tetraphenylporphyrins under Equilibrium Conditions. *J. Org. Chem.* **1987**, *52* (5), 827–836. https://doi.org/10.1021/jo00381a022.

(2) Lee, T.-L.; Duncan, D. A. A Two-Color Beamline for Electron Spectroscopies at Diamond Light Source. *Synchrotron Radiat. News* **2018**, *31* (4), 16–22. https://doi.org/10.1080/08940886.2018.1483653.

(3) Barth, J. V.; Brune, H.; Ertl, G.; Behm, R. J. Scanning Tunneling Microscopy Observations on the Reconstructed Au(111) Surface: Atomic Structure, Long-Range Superstructure, Rotational Domains, and Surface Defects. *Phys. Rev. B* **1990**, *42* (15), 9307–9318. https://doi.org/10.1103/PhysRevB.42.9307.

(4) Wiengarten, A.; Lloyd, J. A.; Seufert, K.; Reichert, J.; Auwärter, W.; Han, R.; Duncan, D. A.; Allegretti, F.; Fischer, S.; Oh, S. C.; Sağlam, Ö.; Jiang, L.; Vijayaraghavan, S.; Écija, D.; Papageorgiou, A. C.; Barth, J. V. Surface-Assisted Cyclodehydrogenation; Break the Symmetry, Enhance the Selectivity. *Chem. – Eur. J.* **2015**, *21* (35), 12285–12290. https://doi.org/10.1002/chem.201502001.

(5) Cirera, B.; de la Torre, B.; Moreno, D.; Ondracek, M.; Zbořil, R.; Miranda, R.; Jelinek, P.; Ecija, D. On-Surface Synthesis of Gold Porphyrins Derivatives via Cascade of Chemical Interactions: Planarization, Self-Metalation and Intermolecular Coupling. *Chem. Mater.* **2019**. https://doi.org/10.1021/acs.chemmater.9b00125.

(6) Lu, J.; Da, B.; Xiong, W.; Du, R.; Hao, Z.; Ruan, Z.; Zhang, Y.; Sun, S.; Gao, L.; Cai, J. Identification and Electronic Characterization of Four Cyclodehydrogenation Products of H2TPP Molecules on Au(111). *Phys. Chem. Chem. Phys.* **2021**, *23* (20), 11784–11788. https://doi.org/10.1039/D1CP01040A.

(7) Mielke, J.; Hanke, F.; Peters, M. V.; Hecht, S.; Persson, M.; Grill, L. Adatoms underneath Single Porphyrin Molecules on Au(111). *J. Am. Chem. Soc.* **2014**, *137* (5), 1844–1849. https://doi.org/10.1021/ja510528x.

(8) Nardi, M.; Verucchi, R.; Corradi, C.; Pola, M.; Casarin, M.; Vittadini, A.; Iannotta, S. Tetraphenylporphyrin Electronic Properties: A Combined Theoretical and Experimental Study of Thin Films Deposited by SuMBD. *Phys. Chem. Chem. Phys.* **2010**, *12* (4), 871–880. https://doi.org/10.1039/B914847G.

(9) Watts, B.; Thomsen, L.; Dastoor, P. C. Methods in Carbon K-Edge NEXAFS: Experiment and Analysis. *J. Electron Spectrosc. Relat. Phenom.* **2006**, *151* (2), 105–120. https://doi.org/10.1016/j.elspec.2005.11.006.

(10) Duncan, D. A.; Deimel, P. S.; Wiengarten, A.; Paszkiewicz, M.; Casado Aguilar, P.; Acres, R. G.; Klappenberger, F.; Auwärter, W.; Seitsonen, A. P.; Barth, J. V.; Allegretti, F. Bottom-Up Fabrication of a Metal-Supported Oxo–Metal Porphyrin. *J. Phys. Chem. C* **2019**, *123* (51), 31011–31025. https://doi.org/10.1021/acs.jpcc.9b08661.

(11) Diller, K.; Klappenberger, F.; Marschall, M.; Hermann, K.; Nefedov, A.; Wöll, Ch.; Barth, J. V. Self-Metalation of 2H-Tetraphenylporphyrin on Cu(111): An x-Ray Spectroscopy Study. *J. Chem. Phys.* **2012**, *136* (1), 014705. https://doi.org/10.1063/1.3674165.